

Advancing Single-Particle Analysis in Synthetic Chemical Systems: A Forward-Looking Discussion

Hui Zhang,* Xiaopeng Li, Jiang Liu, Ya-Qian Lan, and Yu Han*

Single-particle analysis (SPA) is a fundamental method of cryo-electron microscopy developed to resolve the structures of biological macromolecules. This method has seen significant success in structural biology, yet its potential applications in synthetic chemical systems remain underexplored. In this perspective article, SPA and associated electron microscopy techniques are first briefly introduced. It is then proposed that SPA is well-suited for structural analysis of chemical systems where discrete, identical macromolecules can be readily obtained. Applicable systems include various clusters such as coinage metal clusters, metal-oxo/sulfur clusters, metal–organic clusters, and supramolecular compounds like coordination cages and metallo-supramolecular cages. When high-quality large single crystals are unattainable, SPA provides an alternative method for determining their structures. Beyond these end products, it is suggested that SPA can be instrumental in studying synthetic intermediates of materials with specific building units, such as metal–organic frameworks and zeolites. Given that various intermediates coexist in the reaction system, a purification step is necessary before conducting SPA, which can be facilitated by soft-landing electrospray ionization mass spectrometry.

1. Introduction to Single-Particle Analysis

Single-particle analysis (SPA) forms the foundation of cryo-electron microscopy (cryo-EM) technology, which was awarded the Nobel Prize in Chemistry in 2017. Despite this recognition in chemistry, cryo-EM SPA is predominantly applied in structural biology, where it enables the structural determination of biological macromolecules such as proteins and viruses, by analyzing high-resolution transmission electron microscopy (HRTEM) images of numerous individual particles, bypassing the challenge of crystallization into high-quality large single crystals.^[1]

In a typical cryo-EM SPA process, the biological macromolecules of interest are suspended and then rapidly frozen in vitrified ice as single particles for HRTEM imaging. These particles are assumed to be structurally and chemically identical and randomly oriented. Multiple 2D images

are acquired to capture the projections of millions of these particles. Sophisticated algorithms are then employed to categorize and average the images of individual particles based on their orientations, ultimately reconstructing a 3D model of the molecule from the processed images.^[2]

Image processing in SPA is largely automated within the well-established workflow, which includes several key steps: aligning image stacks to correct for beam-induced motion, performing contrast transfer function (CTF) corrections, picking individual particles, and grouping them based on similarity through 2D classification. Subsequent steps involve generating an initial volume as a preliminary estimate of the structure, refining the structure, and identifying possible conformations through 3D classification. The methods developed to accomplish these steps have been comprehensively reviewed in ref. [1c] and they can be implemented using highly integrated software platforms such as RELION,^[3] CryoSPARC,^[4] and EMAN2.^[5]

The SPA technique can now resolve the structures of macromolecules ranging in size from ≈ 50 kilodaltons (kDa) to several megadaltons, comparable to the size range accessible by crystallography. It routinely determines the structures of macromolecules larger than 300 kDa with a resolution better than 3 Å,^[6] and ultrahigh resolutions of <1.5 Å have been achieved in several studies.^[7]

Despite achieving significant success, SPA continues to evolve and improve. For example, SPA reconstruction requires that the

H. Zhang, Y. Han
Center for Electron Microscopy
South China University of Technology
Guangzhou 510640, China
E-mail: huizhang2023@scut.edu.cn; hanyu@scut.edu.cn

H. Zhang, Y. Han
School of Emergent Soft Matter
South China University of Technology
Guangzhou 510640, China

H. Zhang, Y. Han
Guangdong Basic Research Center of Excellence for Energy & Information
Polymer Materials
Guangzhou 510640, China

X. Li
State Key Laboratory of Organometallic Chemistry
Shanghai Institute of Organic Chemistry
Chinese Academy of Sciences
Shanghai 200032, China

X. Li
College of Chemistry and Environmental Engineering
Shenzhen University
Shenzhen 518055, China

J. Liu, Y.-Q. Lan
School of Chemistry
South China Normal University
Guangzhou 510631, China

 The ORCID identification number(s) for the author(s) of this article can be found under <https://doi.org/10.1002/adma.202406914>

DOI: 10.1002/adma.202406914

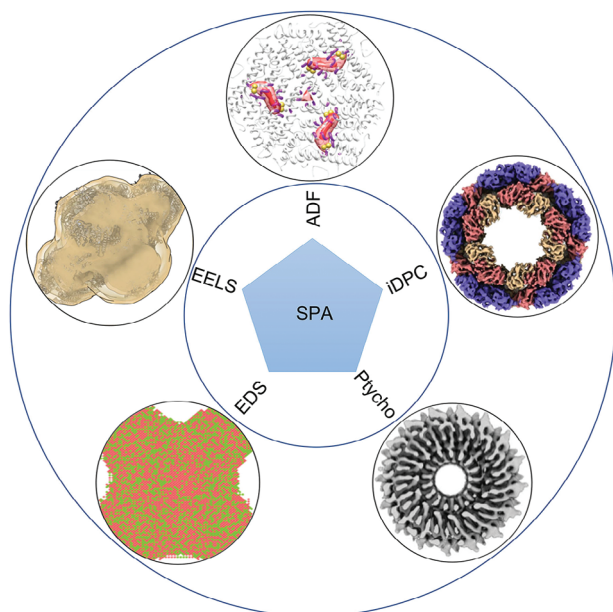


Figure 1. Single-particle analysis using various structural images and spectroscopic maps attained in STEM mode. Ptycho stands for ptychography.

images used for reconstruction accurately represent a monotonic function of the object's projected potential. Traditional HRTEM displays complex image contrasts due to the effects of oscillating CTF and multiple scattering.^[8] These factors can occasionally cause the image contrast to deviate from the ideal situations, potentially leading to the generation of artifacts. This issue can be circumvented by using scanning transmission electron microscopy (STEM) in different modes, such as annular dark field (ADF), integrated differential phase contrast (iDPC), and ptychography, which produce images with simpler contrast mechanisms (Figure 1).

ADF-STEM images are formed using high-angle scattered electrons with chemical sensitivity, and therefore particularly useful for identifying heavy elements. Through SPA utilizing ADF-STEM images isolated Zn and Fe in ferritin are precisely located within the protein cage.^[9] Compared to ADF-STEM, iDPC-STEM offers higher electron dose efficiency and the capability to generate phase-contrast images, making it more suitable for electron beam-sensitive specimens composed of light elements. It employs a segmented detector to measure the center of mass shift of the electron probe, which is related to the electrostatic potentials of the specimen. When iDPC-STEM images of tobacco mosaic virus, recorded with a small convergence angle of 4.0 mrad, were used for SPA reconstructions, the structural determination was achieved at a resolution of 3.5 Å.^[10]

Although the resolution obtained from SPA reconstruction using STEM is currently lower than that using HRTEM, the intrinsic advantage of STEM-based SPA—a simpler CTF that does not require correction—makes it a valuable complement to HRTEM-based SPA in certain situations. However, STEM imaging requires a precisely focused electron probe to achieve high resolution, posing a practical challenge because structural damage is likely to occur during fine focus adjustment if the specimen is sensitive to electron beam irradiation.

Electron ptychography, a computational imaging method, has recently been revitalized due to advancements in electron detector technology. It can be implemented using 4D-STEM data, which essentially comprise a series of convergent beam electron diffraction patterns collected from different positions across a specimen area. From these data, electron ptychography can recover the complex electron wave function at the exit plane of the specimen to produce phase-contrast images.^[11] Compared to conventional STEM, 4D-STEM ptychography boasts several notable advantages, including the ability to attain atomic-resolution images without the need for a focused probe, higher dose efficiency, and greater tolerance to specimen thickness.^[12] Electron ptychography is gathering momentum in the field of structural biology,^[13] as evidenced by recent studies: SPA reconstruction using ptychographic images has achieved a resolution of 5.8 Å for apoferritin protein,^[14] under low-dose conditions of 5–20 electrons per square angstrom ($\text{e}^- \text{Å}^{-2}$), resolutions of 3.5 Å have been realized for biomacromolecules ranging in size from 64 kDa to 4 MDa,^[15] simulations suggest that SPA reconstruction from 2826 ptychograms could achieve a resolution of 2.2 Å for apoferritin.^[16]

Paradoxically, although SPA has gained significant success and the various electron microscopy imaging modalities it relies on are extensively used in the field of chemical materials, the application of SPA itself in chemistry remains quite limited. The primary reason is that particles in chemical systems are typically heterogeneous and do not meet SPA's requirement for identicality. In this perspective article, we aim to emphasize that certain synthetic chemical systems naturally fulfill SPA's requirement for identicality if the specimen is properly prepared,^[17] a fact not widely recognized in the chemical community. Therefore, the established SPA method can be applied for structure determination in such systems. Furthermore, advanced purification techniques can facilitate the extension of SPA to study heterogeneous systems, such as synthetic intermediates. In the following sections, we will explore existing attempts to use SPA for the structural determination of chemical materials and discuss the feasibility of expanding its applications to other synthetic chemical systems.

2. Applications of Single-Particle Analysis in Synthetic Chemical Systems

In the field of materials science, electron tomography (ET) is a commonly utilized technique for the 3D reconstruction of nanoparticles. This method contrasts with the SPA technique, each presenting distinct advantages and drawbacks. ET reconstructs a single particle by collecting a series of images from different projection directions by continuously tilting the specimen. A significant advantage of this approach is that the relative orientations between images are known, thus simplifying the 3D reconstruction process. However, its disadvantages are also evident. It involves repeated exposure of the same particle, accumulating a total electron dose that often reaches the order of $10^6 \text{ e}^- \text{Å}^{-2}$ to achieve atomic resolution,^[18] a level that few samples can withstand without structural damage. Consequently, the application of ET is primarily limited to stable metal nanoparticles. In contrast, SPA reconstructs from a multitude of particles in random orientations without the need for repeated exposures, thereby keeping the electron dose low. Therefore, SPA can be

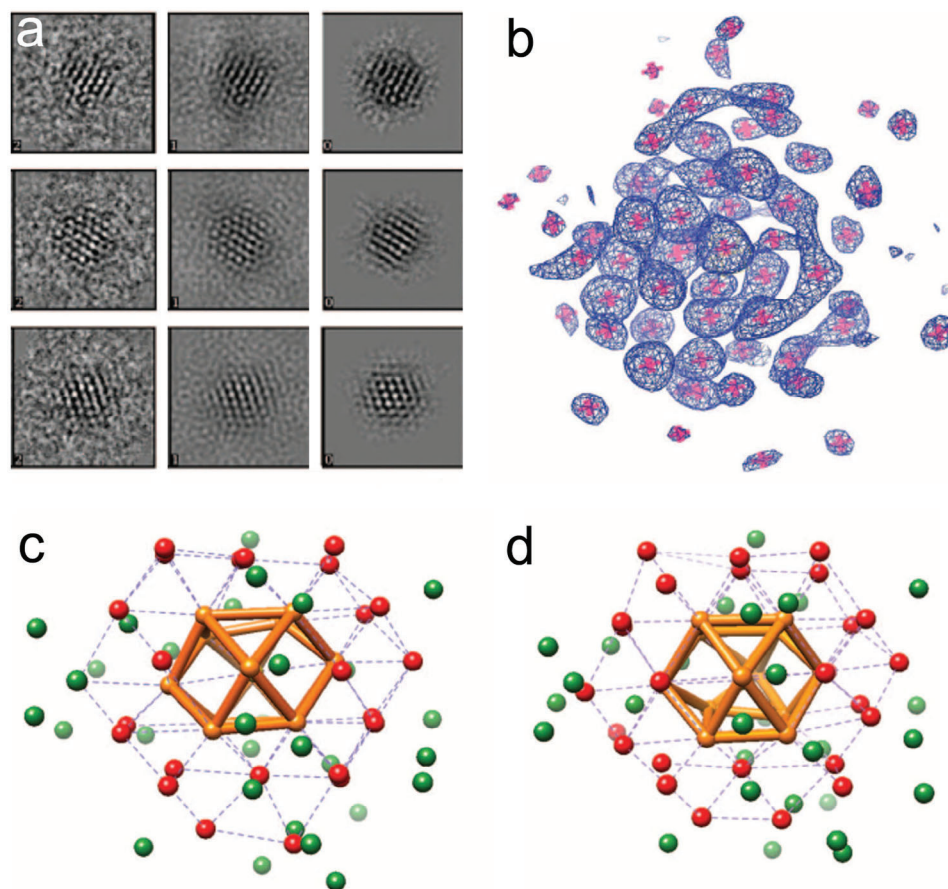


Figure 2. SPA of clusters comprised of 68 gold atoms ($\text{Au}_{68}(\text{SH})_{32}$). a) Representative experimental HRTEM images (left column), class averaged images (middle column), and back-projected images from the 3D reconstruction (right column). b) Electron density map (blue mesh) with the position of gold atoms denoted by pink stars. Atomic configuration reconstructed from SPA c) and relaxed by density functional theory d). Gold atoms forming a cuboctahedron and face-centered cubic (FCC) framework are denoted by orange and red spheres, respectively. Gold atoms with lower symmetry are represented by green balls. Reproduced with permission.^[25] Copyright 2014, AAAS.

used for more materials systems compared to ET in principle. The challenges in SPA are twofold: each particle must be as identical as possible, which imposes high demands on sample preparation; and the relative orientations of the particles are unknown, necessitating more sophisticated reconstruction algorithms.

The present utilization of SPA in chemical material systems remains considerably restricted, with the few existing applications falling into two categories based on the data collection method: reconstruction from a multitude of clusters and reconstruction from a single, randomly rotating particle.

2.1. Reconstruction From a Multitude of Clusters

Coinage metal clusters consist of small aggregates of atoms from coinage metals such as Cu, Ag, and Au. These clusters range in size from a few to several hundred atoms and exhibit unique optical, magnetic, and catalytic properties that are markedly distinct from those of their bulk metal counterparts. The surfaces of these clusters are coated with stabilizing organic ligands, which prevent aggregation, control their sizes, and fine-tune their properties. Notably, coinage metal clusters often form well-

defined structures characterized by specific “magic numbers” of metal atoms and ligands in precise configurations, examples of which include $\text{Au}_{102}(\text{SR})_{44}$,^[19] $\text{Au}_{20}(\text{SR})_{16}$,^[20] $\text{Au}_{25}(\text{SR})_{18}$,^[21] $\text{Au}_{38}(\text{SR})_{24}$,^[22] $\text{Au}_{40}(\text{SR})_{24}$,^[23] and $\text{Au}_{68}(\text{SR})_{34}$.^[24]

While the structures of certain coinage metal clusters have been solved through single-crystal X-ray diffraction, it is often the case that the synthesized clusters do not form large single crystals suitable for this type of structural analysis. Consequently, alternative methods are required to determine their structures. Given that SPA necessitates that the particles under investigation be “identical”, coinage metal clusters are an ideal system for exploration using this method, as each cluster acts as a macro-molecule identical to the others.

The first successful example of employing SPA to determine the atomic structure of a gold cluster (Au_{68}) was reported by Azubel *et al.* in 2014.^[25] In their study, HRTEM images of 939 particles were utilized for 3D reconstruction, achieving a resolution of 2.4 Å. The back-projected images from the reconstructed volume aligned well with the 2D HRTEM images, confirming the high accuracy of the reconstruction (Figure 2a,b). Analysis of the reconstruction results revealed that the cluster comprises three structural domains: a cuboctahedron core made up of 13 Au

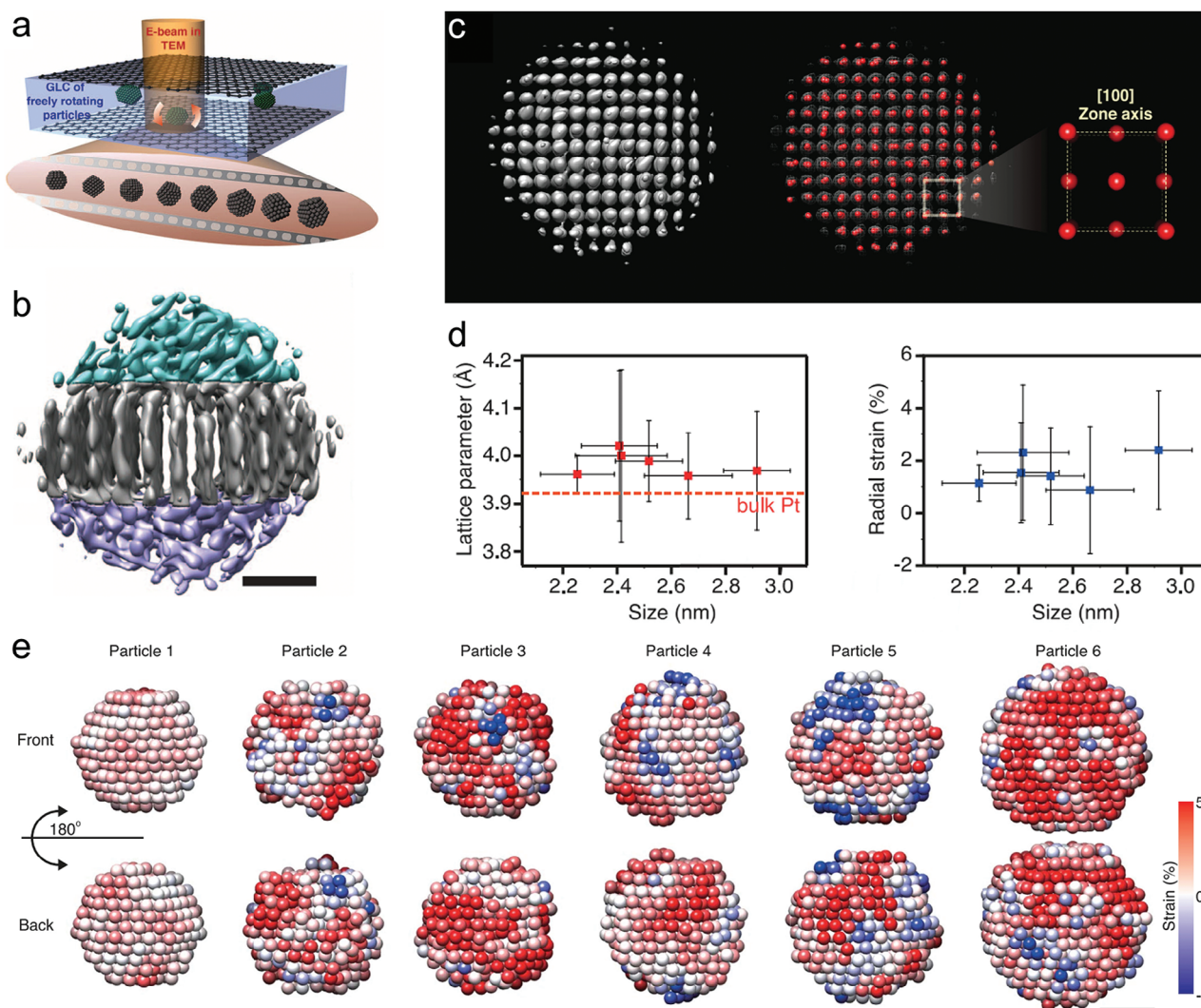


Figure 3. Schematic illustration of the experimental setup for the Brownian one-particle method a). Pt nanocrystals in the graphene liquid cell rotate freely. b) 3D density maps calculated from an individual Pt nanoparticle. Three distinct domains were identified and denoted by blue, gray, and purple. The nanoparticle was oriented to expose {111} planes of the core domain. Scale bar: 0.5 nm. Reproduced with permission.^[27] Copyright 2015, AAAS. c) Atomic resolution 3D density map (left) and atomic positions (right) along [100]. Red balls denote Pt atoms. d) Lattice parameters and averaged radial strain of Pt nanoparticles calculated from the reconstructed 3D structures. e) Radial strain maps of six nanoparticles with different sizes. Scale bar: 1 nm. Reproduced with permission.^[28] Copyright 2020, AAAS.

atoms, a near-core region where 24 Au atoms form an FCC-like framework, and a peripheral region with 31 Au atoms deviating from the standard FCC packing (Figure 2c,d). Later, they applied the same approach to solve the structure of $\text{Au}_{144}(\text{3-MBA})_x$ and discovered that the atoms near the surface deviate from the FCC configuration, resulting in the curvature of the particle.^[26] Overall, the SPA method used in this work is fundamentally the same as the SPA used in structural biology; the only difference lies in the subjects of study.

2.2. Reconstruction From a Single Rotating Particle

Unlike coinage metal clusters with precise “magic numbers”, metallic nanocrystals, even synthesized from the same batch,

are typically heterogeneous, lacking uniform particle sizes (atom numbers) and consistent surface atomic arrangements. Conventional SPA cannot be directly applied to investigate such systems due to the difficulty in obtaining a sufficient population of identical particles.

In 2015, Park and colleagues developed a novel data acquisition strategy utilizing the freedom of particles in solution to achieve atomic-resolution 3D reconstruction of a Pt nanocrystal.^[27] Specifically, instead of tilting the specimen, they acquired a time series of HRTEM images for a selected nanocrystal in varying orientations due to its Brownian motion in liquid (Figure 3a). The acquired images are equivalent to the images from numerous identical particles in conventional SPA, and consequently, the established SPA method can be applied. From the perspective of data collection, this method is similar to ET, while

from the standpoint of data processing, it aligns with SPA. Detailed technical descriptions of this method, termed “Brownian one-particle,” were provided later in ref. [29]. Since this method involves repeated exposure of a single particle, it shares the same limited application scope as ET and can only be used for highly stable particles.

In the first demonstration of the Brownian one-particle reconstruction, a resolution of 2.10 Å was achieved for a Pt nanocrystal.^[27] The results revealed the existence of three distinct domains having different orientations (Figure 3b). By improving data processing methods, such as incorporating motion corrections and background subtraction, the resolution was further enhanced to greater than 0.72 Å. This resolution enables the localization of every atom within the nanoparticles (Figure 3c) and the identification of structural features that are unattainable by other methods.^[28] The reconstruction reveals that Pt nanocrystals coated with polyvinyl pyrrolidone (PVP) have an expanded lattice relative to the bulk (Figure 3d,e).^[30] This observation contrasts with the lattice compressions theoretically expected in metal nanocrystals without protective ligands. Subsequently, Park and colleagues found that individual Pt nanoparticles exhibit inherent heterogeneity, characterized by a range of dynamic and irregular surface structures and the exposure of various facets.^[31]

3. Perspective

3.1. Synthetic Chemical Systems Suitable for SPA

Experimental demonstrations of atomic-resolution SPA are currently limited to single-element metallic clusters and nanocrystals, as discussed earlier. Its significant potential for application to other synthetic chemical systems has been largely overlooked. We contend that SPA is suited for the structural analysis of chemical materials composed of identical, structurally rigid macromolecular building units. These units assemble into materials through weak intermolecular forces such as Van der Waals interactions, while the materials can be dissociated back into individual discrete units with intact structural integrity under specific conditions, such as dissolution. If the materials cannot grow into large single crystals suitable for structural solution using X-ray diffraction, SPA could serve as an alternative tool to investigate their structures.

In addition to the coinage metal clusters discussed earlier, numerous synthetic chemical systems meet this requirement. Examples include various high-nuclearity clusters, such as metal-oxo/sulfur clusters and metal–organic clusters, as well as supramolecular compounds like coordination cages and metallo-supramolecular cages. Unlike biological macromolecules, the units of many of these materials can be isolated from the solvent as stable “particles” without the need for using vitrified ice to preserve their native states. Consequently, their SPA does not necessitate solvent involvement or cryogenic conditions. Moreover, many of these particles contain metal elements, which enhance image contrast. These factors potentially simplify data acquisition and analysis compared to the application of SPA in biology.

Taking metal-oxo/sulfur cluster materials as examples,^[32] the functional properties of these materials significantly vary depending on the structure of the clusters. However, achieving or-

dered assembly of these clusters to produce large single crystals is challenging. Moreover, the crystals formed often contain defects such as twinning and local disorder. Consequently, solving the structure of these materials using diffraction methods seldom meets crystallographic standards. On the other hand, these materials can be dissolved in organic solvents^[17a,b] or water,^[33] producing discrete identical clusters (Figure 4a,b). This characteristic renders SPA a powerful method for determining their structures.

Another example of crystal-size limiting structural determination is coordination cages, which have garnered significant attention in the field of supramolecular chemistry and materials science.^[34] The molecular structures, including the arrangement of atoms and conformational orientation of molecular backbones, are of paramount importance for the rational design of new materials with molecular-level precision. As the crystals, particularly for large macromolecules and supramolecules containing extensive voids filled with disordered solvent molecules or ions, are usually too small to be analyzed by diffraction methods, TEM imaging is the optimal choice for structural determination. For instance, a 10-nm-sized cuboctahedron metallo-cages and well-ordered square arrays of assembled cuboctahedra were recently visualized by 2D single particle analysis.^[17c] Similar to crystalline high-nuclearity clusters, the crystals of coordination cages can also be disassembled into individual well-defined clusters (Figure 4c).^[35] As such, structural analysis of these molecular architectures at the single-molecule level can be facilitated by SPA.

3.2. Potential Applications of SPA for Synthetic Intermediates

The materials discussed above that are potential candidates for structural determination using SPA are the end products of synthetic chemical systems. In addition to these end products, we believe that SPA can also be applied to resolve the structures of some intermediate products in the synthesis process. Nanoporous crystalline materials, such as inorganic zeolites and metal–organic frameworks (MOFs), are composed of primary and secondary building units. These units are often defined conceptually to simplify the description and enhance the understanding of their structures, although some may also exist as actual intermediates within synthetic systems. Currently, there is a lack of effective tools for directly observing these synthetic intermediates. Attempts to use in situ liquid TEM to investigate intermediates in the synthesis of MOFs have provided some insights. These include observing the evolution of Hf-based clusters into dimers, trimers, multimers, and a disordered structure,^[38] as well as identifying Hf₆ and Hf₁₂ clusters at the early stages of synthesis for UiO-67 and hcp-UiO-67 (hcp: hexagonal close-packed), respectively.^[39] However, conventional in situ liquid TEM is incapable of revealing the 3D structures of these intermediates.

The primary challenge of using SPA to study synthetic intermediates is that these intermediates often consist of mixtures of different species. Although Brownian one-particle SPA can theoretically handle heterogeneous populations, it is not suitable for this purpose due to the high electron doses required. This is problematic because intermediates are generally sensitive to electron beam exposure. We propose that combining a sample

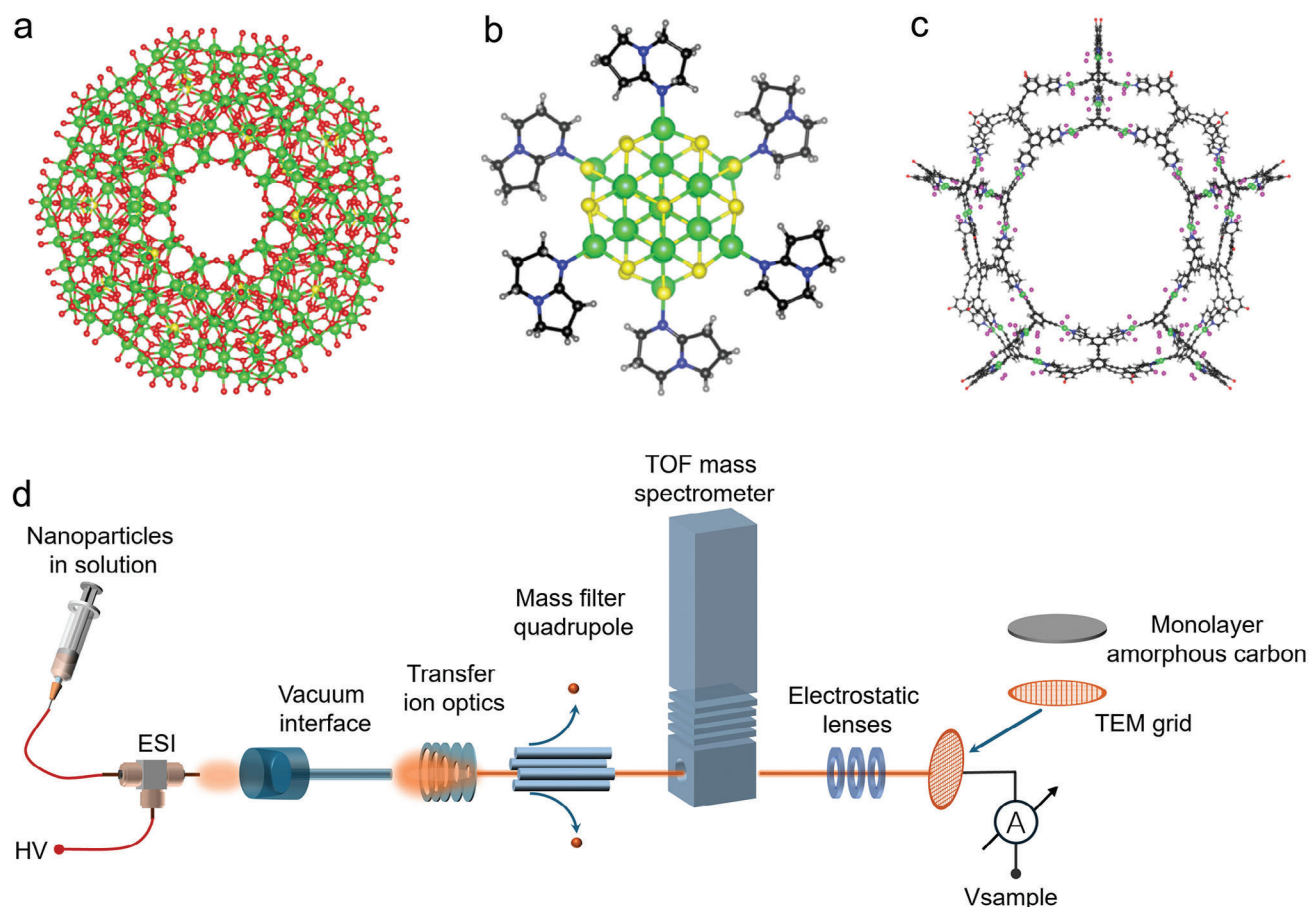


Figure 4. Clusters and separation method. a) $\text{Mo}_{240}\text{O}_{740}\text{S}_{32}$ cluster.^[17a] Green, red, and yellow balls denote Mo, O, and S atoms, respectively. b) $\text{In}_{20}\text{S}_{33}$ cluster.^[36] In, S, N, C, and H are represented by green, yellow, blue, black, and grey balls, respectively. c) $\text{C}_{1800}\text{H}_{2370}\text{O}_{210}\text{N}_{60}\text{F}_{180}\text{P}_{120}\text{S}_{60}\text{Pt}_{60}$ coordination cage.^[37] Pt, P, O, N, C, and H are represented by green, purple, red, blue, black, and grey balls, respectively. F and S are not shown here for brevity. d) Schematic illustration of particle purification using soft-landing electrospray ionization mass spectrometry. The process includes several steps: i) electrospray ionizes the particles, producing a beam of charged particles; ii) the beam enters the vacuum interface through a heated metal capillary and is collimated in an ion funnel by a collisional collimation quadrupole; iii) the interested region of m/z monitored by the time-of-flight mass spectrometer is selected by a mass filtering quadrupole; iv) the selected particles are then guided by electrostatic lenses and deposited on a TEM grid. Soft landing of selected particles is managed by reducing the kinetic energy of the charged nanoparticles to a few eV per charge via applying a bias voltage to the grid.

preparation technique with the standard SPA could offer a solution to this challenge. This strategy has proven effective when used for biomacromolecules.^[40] Specifically, soft-landing electrospray ionization mass spectrometry can be employed to isolate the intermediate of interest from the synthetic system, as shown in Figure 4d.^[41] The mass-charge ratio (m/z) of the ionized species is monitored by the mass spectrometer and the target species are selected by a mass filtering quadrupole and deposited onto TEM grids. These grids are ideally composed of monolayer amorphous carbon^[42] or, alternatively, graphene to reduce background signals in the images used for SPA.

3.3. Emerging Imaging Modalities for SPA

As previously outlined, images utilized for SPA can be acquired through various imaging modalities, such as HRTEM, ADF-STEM, iDPC-STEM, and ptychography. Table 1 summarizes the

characteristics of these techniques as well as the Brownian one-particle method for comparison. Since the efficacy of SPA largely hinges on image quality, particularly the signal-to-noise ratio (SNR), ADF-STEM may be considered a last resort due to its lower SNR for a given dose compared to other imaging modalities. Considering that HRTEM-based SPA is well-established and ptychography offers superior resolution and SNR compared to iDPC-STEM,^[43] the following discussions will focus on the potential application of the emerging electron ptychography technique in SPA for challenging synthetic chemical systems.

Compared to HRTEM, electron ptychography offers several advantages. First, ptychography avoids the issue of CTF oscillation present in HRTEM, making the obtained images easier to process. Second, ptychography provides better information transfer. HRTEM images typically require a large defocus to enhance information transfer at low spatial frequencies, which results in a loss of structural information at higher spatial frequencies. In contrast, electron ptychography can continuously recover the

Table 1. Comparison of SPA reconstructions using various techniques.

	Requirement for homogeneity	State-of-the-art resolution @ electron dose used*	Required focus conditions
Brownian one-particle (HRTEM)	No	0.72 Å @ $>10^5$ e ⁻ Å ⁻² [28,29b,31a]	In-focus or requiring CTF correction
HRTEM	Yes	1.09 Å @ 40 e ⁻ Å ⁻² [14]	In-focus or requiring CTF correction
ADF		21 Å @ 229 e ⁻ Å ⁻² [9]	In-focus
iDPC		3.5 Å @ 35 e ⁻ Å ⁻² [10]	In-focus
Ptychography		Experiment: 5.8 Å @ 35 e ⁻ Å ⁻² [14] Simulation: 2.9 Å @ 20 e ⁻ Å ⁻² [15] 2.2 Å @ 73 e ⁻ Å ⁻² [16]	No requirements
EDS		7 Å @ 2×10^6 e ⁻ Å ⁻² [48]	In-focus
EELS		4 nm @ 92 e ⁻ Å ⁻² [49]	In-focus
EFTEM		4 nm @ 2000 e ⁻ Å ⁻² [51]	Unexplored

* The resolution presented is obtained from different types of samples and therefore not directly comparable.

phase of the object over a wide range of spatial frequencies.^[44] Third, ptychography delivers images with improved SNR. For example, the SNR in ptychograms has been demonstrated to be two orders of magnitude higher than that of HRTEM at 0.5 Å⁻¹ with a dose of 20 e⁻ Å⁻².^[15] Lastly, ptychographic SPA can eliminate the image shift caused by irradiation using well-established algorithms to remove probe position errors in the iteration process.^[45]

The best resolutions achieved by ptychographic SPA to date are 5.8 Å in experiments^[14] and 2.2 Å in simulations.^[16] The inferior spatial resolution compared to conventional SPA is likely due to the use of small convergence semi-angles (≈ 5 mrad) for data collection and the lack of correction for beam-induced sample motion during reconstruction.^[14,16,46] Recently, a carbon nanotube encapsulating a complex ZrTe sandwich structure has been resolved at atomic resolution using electron ptychography combined with electron tomography.^[47] Given the similarities between tomography and SPA, and the ongoing advancements in 4D-STEM detectors and ptychographic reconstruction algorithms, we are optimistic about achieving atomic-resolution ptychographic SPA.

3.4. Compositional SPA for Multi-Element Systems

Compared to single-element materials, the structural analysis of materials containing multiple elements is more challenging. Although ptychography is element sensitive, the element assignment of each atom is nontrivial. This task would be simplified if compositional information were simultaneously obtained using energy dispersive spectroscopy (EDS) or electron energy loss spectroscopy (EELS). Single-particle reconstruction of EDS data collected from randomly oriented PtNi nanoparticles revealed a Pt-rich core, a Ni-rich hollow octahedral intermediate shell, and a Pt-rich rhombic dodecahedral skeleton framework at a resolution of 7 Å (Figure 1).^[48] EELS data from the rabbit ryanodine receptor have been utilized for SPA reconstruction, achieving a resolution of ≈ 4 nm and enabling the localization of specific domains (Figure 1).^[49] Energy-filtered TEM (EFTEM) serves as an alternative to EELS spectrum imaging in SPA. While EFTEM utilizing zero-loss signals has been widely employed in SPA of biological samples to improve image contrast and reconstruction resolution,^[50] SPA based on core-loss signals,^[51] which

holds promise for multi-element materials, remains largely unexplored.

The scattering cross-section of signals used for EDS and EELS is several orders of magnitude lower compared to those used for imaging. Due to the weak signal, the single-particle reconstruction of spectroscopic datasets currently requires support from structural images. These images facilitate the generation of particle coordinates and reconstruction poses for the spectroscopic data. Even so, achieving atomic resolution reconstruction using spectroscopic data remains exceedingly difficult. With advancements in the development of high-performance X-ray and electron detectors and more powerful reconstruction algorithms, the electron dose required by EDS/EELS SPA is expected to be reduced, while the reconstruction resolution is expected to improve. Consequently, EDS/EELS SPA holds the potential to further enrich our understanding of various nanostructures in synthetic chemical systems and beyond.

4. Summary

SPA is a powerful technique based on TEM for 3D structural determination. Although SPA has achieved significant success in the field of biology, its application in chemical material systems remains largely underutilized. One of the major challenges in applying SPA to chemical systems is particle heterogeneity, a problem that persists even in some biological systems despite decades of development.

This perspective emphasizes to the chemical community that certain synthetic chemical systems can attain the necessary particle homogeneity, thus enabling structural studies using SPA. SPA is particularly well-suited for the structural analysis of chemical systems where discrete, identical macromolecules can be readily obtained. Notable examples include various clusters such as coinage metal clusters, metal-oxo/sulfur clusters, metal-organic clusters, and supramolecular compounds like coordination cages and metallo-supramolecular cages.

Through the use of purification techniques, such as soft-landing electrospray ionization mass spectrometry, SPA can be applied to a broader range of chemical systems. This includes synthetic intermediates of materials with specific building units, such as metal-organic frameworks and zeolites. With the integration of emerging imaging and spectroscopic modalities into

SPA, it is anticipated that SPA will find remarkable applications in synthetic chemical systems.

Acknowledgements

H. Z. thanks the support from the Fundamental Research Funds for the Central Universities (No. D2230330). X. L. acknowledges the Developmental Fund for Science and Technology of Shenzhen (JCYJ20220818095615032) and the Guangdong Province "Pearl River Talents Plan" Innovative and Entrepreneurial Teams Project (2021ZT09C289).

Conflict Of Interest

The authors declare no conflict of interest.

Keywords

coordination cage, metal–organic framework, ptychography, single particle analysis

Received: May 15, 2024

Revised: July 30, 2024

Published online:

- [1] a) E. Nogales, *Nat. Methods* **2016**, *13*, 24; b) D. Lyumkis, *J. Biol. Chem.* **2019**, *294*, 5181; c) J. L. Vilas, J. M. Carazo, C. O. S. Sorzano, *Chem. Rev.* **2022**, *122*, 13915; d) J. Frank, *Microscopy* **2016**, *65*, 3.
- [2] a) X. Yu, L. Jin, Z. H. Zhou, *Nature* **2008**, *453*, 415; b) X. Zhang, E. Settembre, C. Xu, P. R. Dormitzer, R. Bellamy, S. C. Harrison, N. Grigorieff, *Proc. Natl. Acad. Sci.* **2008**, *105*, 1867; c) W. Jiang, M. L. Baker, J. Jakana, P. R. Weigele, J. King, W. Chiu, *Nature* **2008**, *451*, 1130.
- [3] S. H. W. Scheres, *J. Mol. Biol.* **2012**, *415*, 406.
- [4] A. Punjani, J. L. Rubinstein, D. J. Fleet, M. A. Brubaker, *Nat. Methods* **2017**, *14*, 290.
- [5] G. Tang, L. Peng, P. R. Baldwin, D. S. Mann, W. Jiang, I. Rees, S. J. Ludtke, *J. Struct. Biol.* **2007**, *157*, 38.
- [6] a) M. Khoshouei, M. Radjainia, W. Baumeister, R. Danev, *Nat. Commun.* **2017**, *8*, 16099; b) A. Bartsaghi, C. Aguerrebere, V. Falconieri, S. Banerjee, L. A. Earl, X. Zhu, N. Grigorieff, J. L. S. Milne, G. Sapiro, X. Wu, S. Subramaniam, *Structure* **2018**, *26*, 848.
- [7] a) K. M. Yip, N. Fischer, E. Paknia, A. Chari, H. Stark, *Nature* **2020**, *587*, 157; b) S. Maki-Yonekura, K. Kawakami, K. Takaba, T. Hamaguchi, K. Yonekura, *Commun. Chem.* **2023**, *6*, 98; c) T. Nakane, A. Kotecha, A. Sente, G. McMullan, S. Masiulis, P. M. G. E. Brown, I. T. Grigoras, L. Malinauskaite, T. Malinauskas, J. Miehl, T. Uchański, L. Yu, D. Karia, E. V. Pechnikova, E. de Jong, J. Keizer, M. Bischoff, J. McCormack, P. Tiemeijer, S. W. Hardwick, D. Y. Chirgadze, G. Murshudov, A. R. Aricescu, S. H. W. Scheres, *Nature* **2020**, *587*, 152.
- [8] D. Ren, C. Ophus, M. Chen, L. Waller, *Ultramicroscopy* **2020**, *208*, 112860.
- [9] N. Elad, G. Bellapadrona, L. Houben, I. Sagi, M. Elbaum, *Proc. Natl. Acad. Sci.* **2017**, *114*, 11139.
- [10] I. Lazić, M. Wirix, M. L. Leidl, F. de Haas, D. Mann, M. Beckers, E. V. Pechnikova, K. Müller-Caspary, R. Egoavil, E. G. T. Bosch, C. Sachse, *Nat. Methods* **2022**, *19*, 1126.
- [11] a) A. M. Blackburn, R. A. McLeod, *Microscopy* **2021**, *70*, 131; b) C. Ophus, *Microsc. Microanal.* **2019**, *25*, 563.
- [12] P. Li, A. Maiden, *Sci. Rep.* **2018**, *8*, 2049.
- [13] C. Huang, J. S. Kim, A. I. Kirkland, *Curr. Opin. Struct. Biol.* **2023**, *83*, 102730.
- [14] B. Küçükoğlu, I. Mohammed, R. C. Guerrero-Ferreira, S. M. Ribet, G. Varnavides, M. L. Leidl, K. Lau, S. Nazarov, A. Myasnikov, C. Sachse, K. Müller-Caspary, C. Ophus, H. Stahlberg, *bioRxiv* **2024**, <https://doi.org/10.1101/2024.02.12.579607>.
- [15] P. M. Pelz, W. X. Qiu, R. Bücker, G. Kassier, R. J. D. Miller, *Sci. Rep.* **2017**, *7*, 9883.
- [16] X. Pei, L. Zhou, C. Huang, M. Boyce, J. S. Kim, E. Liberti, Y. Hu, T. Sasaki, P. D. Nellist, P. Zhang, D. I. Stuart, A. I. Kirkland, P. Wang, *Nat. Commun.* **2023**, *14*, 3027.
- [17] a) J. Lin, N. Li, S. Yang, M. Jia, J. Liu, X. M. Li, L. An, Q. Tian, L. Z. Dong, Y. Q. Lan, *J. Am. Chem. Soc.* **2020**, *142*, 13982; b) J. Liu, N. Jiang, J. M. Lin, Z. B. Mei, L. Z. Dong, Y. Kuang, J. J. Liu, S. J. Yao, S. L. Li, Y. Q. Lan, *Angew. Chem., Int. Ed.* **2023**, *62*, 202304728; c) L. He, H. K. Hsu, L. Li, L. T. Lin, T. H. Tu, T. G. Ong, G. G. Liou, Y. T. Chan, *Chem* **2022**, *8*, 494.
- [18] a) M. C. Scott, C. C. Chen, M. Mecklenburg, C. Zhu, R. Xu, P. Ercius, U. Dahmen, B. C. Regan, J. Miao, *Nature* **2012**, *483*, 444; b) S. Moniri, Y. Yang, J. Ding, Y. Yuan, J. Zhou, L. Yang, F. Zhu, Y. Liao, Y. Yao, L. Hu, P. Ercius, J. Miao, *Nature* **2023**, *624*, 564; c) Y. Yuan, D. S. Kim, J. Zhou, D. J. Chang, F. Zhu, Y. Nagaoka, Y. Yang, M. Pham, S. J. Osher, O. Chen, P. Ercius, A. K. Schmid, J. Miao, *Nat. Mater.* **2022**, *21*, 95.
- [19] P. D. Jadzinsky, G. Calero, C. J. Ackerson, D. A. Bushnell, R. D. Kornberg, *Science* **2007**, *318*, 430.
- [20] M. Zhu, H. Qian, R. Jin, *J. Am. Chem. Soc.* **2009**, *131*, 7220.
- [21] M. W. Heaven, A. Dass, P. S. White, K. M. Holt, R. W. Murray, *J. Am. Chem. Soc.* **2008**, *130*, 3754.
- [22] H. Qian, W. T. Eckenhoff, Y. Zhu, T. Pintauer, R. Jin, *J. Am. Chem. Soc.* **2010**, *132*, 8280.
- [23] H. Qian, Y. Zhu, R. Jin, *J. Am. Chem. Soc.* **2010**, *132*, 4583.
- [24] A. Dass, *J. Am. Chem. Soc.* **2009**, *131*, 11666.
- [25] M. Azubel, J. Koivisto, S. Malola, D. Bushnell, G. L. Hura, A. L. Koh, H. Tsunoyama, T. Tsukuda, M. Pettersson, H. Häkkinen, R. D. Kornberg, *Science* **2014**, *345*, 909.
- [26] M. Azubel, A. L. Koh, K. Koyasu, T. Tsukuda, R. D. Kornberg, *ACS Nano* **2017**, *11*, 11866.
- [27] J. Park, H. Elmlund, P. Ercius, J. M. Yuk, D. T. Limmer, Q. Chen, K. Kim, S. H. Han, D. A. Weitz, A. Zettl, A. P. Alivisatos, *Science* **2015**, *349*, 290.
- [28] B. H. Kim, J. Heo, S. Kim, C. F. Reboul, H. Chun, D. Kang, H. Bae, H. Hyun, J. Lim, H. Lee, B. Han, T. Hyeon, A. P. Alivisatos, P. Ercius, H. Elmlund, *J. Park, Science* **2020**, *368*, 60.
- [29] a) B. H. Kim, J. Heo, J. Park, *Small Sci* **2021**, *1*, 2000045; b) C. F. Reboul, J. Heo, C. Machello, S. Kiesewetter, B. H. Kim, S. Kim, D. Elmlund, P. Ercius, J. Park, H. Elmlund, *Sci. Adv.* **2021**, *7*, eabe6679.
- [30] J. Heo, D. Kang, S. Kim, H. Chun, B. Han, B. H. Kim, J. Park, *Chem-NanoMat* **2022**, *8*, 202200057.
- [31] a) H. Wietfeldt, R. Meana-Pañeda, C. Machello, C. F. Reboul, C. T. S. Van, S. Kim, J. Heo, B. H. Kim, S. Kang, P. Ercius, J. Park, H. Elmlund, *Commun. Chem.* **2024**, *7*, 4; b) S. Kim, J. Kwag, C. Machello, S. Kang, J. Heo, C. F. Reboul, D. Kang, S. Kang, S. Shim, S. J. Park, B. H. Kim, T. Hyeon, P. Ercius, H. Elmlund, J. Park, *Nano Lett.* **2021**, *21*, 1175.
- [32] a) C. Sun, B. K. Teo, C. Deng, J. Lin, G. G. Luo, C. H. Tung, D. Sun, *Coord. Chem. Rev.* **2021**, *427*, 213576; b) M. Nyman, P. C. Burns, *Chem. Soc. Rev.* **2012**, *41*, 7354; c) S. Lee, H. Jeong, D. Nam, M. S. Lah, W. Choe, *Chem. Soc. Rev.* **2021**, *50*, 528; d) X. M. Luo, Y. K. Li, X. Y. Dong, S. Q. Zang, *Chem. Soc. Rev.* **2023**, *52*, 383.
- [33] a) O. Sadeghi, C. Falaise, P. I. Molina, R. Hufschmid, C. F. Campana, B. C. Noll, N. D. Browning, M. Nyman, *Inorg. Chem.* **2016**, *55*, 11078; b) M. Nyman, T. M. Alam, *J. Am. Chem. Soc.* **2012**, *134*, 20131; c) S. Goberna-Ferrón, D. H. Park, J. M. Amador, D. A. Keszler, M. Nyman, *Angew. Chem., Int. Ed.* **2016**, *55*, 6221.

- [34] a) R. Chakrabarty, P. S. Mukherjee, P. J. Stang, *Chem. Rev.* **2011**, *111*, 6810; b) D. Fujita, Y. Ueda, S. Sato, N. Mizuno, T. Kumasaka, M. Fujita, *Nature* **2016**, *540*, 563; c) H. Wang, Y. Li, N. Li, A. Filosa, X. Li, *Nat. Rev. Mater.* **2021**, *6*, 145; d) J. Guo, P. C. Mayers, G. A. Breault, C. A. Hunter, *Nat. Chem.* **2010**, *2*, 218.
- [35] a) E. G. Percástegui, T. K. Ronson, J. R. Nitschke, *Chem. Rev.* **2020**, *120*, 13480; b) K. Byrne, M. Zubair, N. Zhu, X. P. Zhou, D. S. Fox, H. Zhang, B. Twamley, M. J. Lennox, T. Düren, W. Schmitt, *Nat. Commun.* **2017**, *8*, 15268.
- [36] L. Sun, H. Y. Zhang, J. Zhang, Y. J. Jia, Y. Z. Yu, J. J. Hou, Y. X. Wang, X. M. Zhang, *Dalton Trans.* **2020**, *49*, 13958.
- [37] H. Wang, L. P. Zhou, Y. Zheng, K. Wang, B. Song, X. Yan, L. Wojtas, X. Q. Wang, X. Jiang, M. Wang, Q. F. Sun, B. Xu, H. B. Yang, A. C. H. Sue, Y. T. Chan, J. L. Sessler, Y. Jiao, P. J. Stang, X. Li, *Angew. Chem., Int. Ed.* **2021**, *60*, 1298.
- [38] X. Peng, P. M. Pelz, Q. Zhang, P. Chen, L. Cao, Y. Zhang, H. G. Liao, H. Zheng, C. Wang, S. G. Sun, M. C. Scott, *Nat. Commun.* **2022**, *13*, 5197.
- [39] P. Chen, Z. Tang, Z. Zeng, X. Hu, L. Xiao, Y. Liu, X. Qian, C. Deng, R. Huang, J. Zhang, Y. Bi, R. Lin, Y. Zhou, H. Liao, D. Zhou, C. Wang, W. Lin, *Matter* **2020**, *2*, 1651.
- [40] J. N. Longchamp, S. Rauschenbach, S. Abb, C. Escher, T. Latychevskaia, K. Kern, H. W. Fink, *Proc. Nat. Acad. Sci.* **2017**, *114*, 1474.
- [41] T. Chen, Q. Yao, R. R. Nasaruddin, J. Xie, *Angew. Chem., Int. Ed.* **2019**, *58*, 11967.
- [42] C. T. Toh, H. Zhang, J. Lin, A. S. Mayorov, Y. P. Wang, C. M. Orofeo, D. B. Ferry, H. Andersen, N. Kakenov, Z. Guo, I. H. Abidi, H. Sims, K. Suenaga, S. T. Pantelides, B. Özyilmaz, *Nature* **2020**, *577*, 199.
- [43] a) H. Sha, J. Cui, J. Li, Y. Zhang, W. Yang, Y. Li, R. Yu, *Sci. Adv.* **2023**, *9*, eadf1151; b) Z. Chen, Y. Jiang, Y. T. Shao, M. E. Holtz, M. Odstrčil, M. Guizar-Sicairos, I. M. Schulze-Jonack, S. Ganschow, D. G. Schlom, D. A. Muller, *Microsc. Microanal.* **2022**, *28*, 376; c) H. Zhang, G. Li, J. Zhang, D. Zhang, Z. Chen, X. Liu, P. Guo, Y. Zhu, C. Chen, L. Liu, X. Guo, Y. Han, *Science* **2023**, *380*, 633.
- [44] L. Zhou, J. Song, J. S. Kim, X. Pei, C. Huang, M. Boyce, L. Mendonça, D. Clare, A. Siebert, C. S. Allen, E. Liberti, D. Stuart, X. Pan, P. D. Nellist, P. Zhang, A. I. Kirkland, P. Wang, *Nat. Commun.* **2020**, *11*, 2773.
- [45] a) A. M. Maiden, M. J. Humphry, M. C. Sarahan, B. Kraus, J. M. Rodenburg, *Ultramicroscopy* **2012**, *120*, 64; b) S. Ning, W. Xu, L. Loh, Z. Lu, M. Bosman, F. Zhang, Q. He, *Ultramicroscopy* **2023**, *248*, 113716; c) A. Lin, P. Sheng, S. Ning, F. Zhang, *Appl. Opt.* **2024**, *63*, 804.
- [46] Y. Yu, K. A. Spoth, M. Colletta, K. X. Nguyen, S. E. Zeltmann, X. S. Zhang, M. Paraan, M. Kopylov, C. Dubbeldam, D. Serwas, H. Siems, D. A. Muller, L. F. Kourkoutis, *bioRxiv* **2024**, <https://doi.org/10.1101/2024.04.22.590491>.
- [47] P. M. Pelz, S. M. Griffin, S. Stonemeyer, D. Popple, H. DeVylde, P. Ercius, A. Zettl, M. C. Scott, C. Ophus, *Nat. Commun.* **2023**, *14*, 7906.
- [48] Y. C. Wang, T. J. A. Slater, G. M. Leteba, A. M. Roseman, C. P. Race, N. P. Young, A. I. Kirkland, C. I. Lang, S. J. Haigh, *Nano Lett.* **2019**, *19*, 732.
- [49] O. Pfeil-Gardiner, H. V. D. Rosa, D. Riedel, Y. S. Chen, D. Lörks, P. Kükellhan, M. Linck, H. Müller, F. V. Petegem, B. J. Murphy, *Nat. Methods* **2024**, in press.
- [50] a) R. R. Schröder, *J. Microsc.* **1992**, *166*, 389; b) K. Yonekura, M. B. Braunfeld, S. Maki-Yonekura, D. A. Agard, *J. Struct. Biol.* **2006**, *156*, 524.
- [51] D. R. Beniac, G. J. Czarnota, B. L. Rutherford, F. P. Ottensmeyer, G. Harauz, *J. Microsc.* **1997**, *188*, 24.